

## Robust Automated detection of Nanocarriers' Toxicity using Microscopic Image Analysis

B. Saini<sup>1,\*</sup>, S. Srivastava<sup>1</sup> and A.K. Bajpai<sup>2</sup>

<sup>1</sup>School of Computing and Information Technology, Manipal University Jaipur, India

<sup>2</sup>Bose Memorial Research Laboratory, Department of Chemistry, Government Autonomous Science College, Jabalpur (MP), India

### Abstract

Nanocarriers' usage turned out to be a revolutionizing factor in the field of medical diagnosis and therapies. One of these therapies includes drug delivery system, where the nanocarriers are utilized for targeted and controlled delivery of drug to the diseased sites. Toxicity is one of the crucial issues which can arise during this process and needs to be addressed seriously and as early as possible. This paper reports an automated system for the relatively new and undiscovered area, where cell detection and evaluation play a major role in toxicity prediction of nanocarriers during the drug delivery process. The toxicity level was decided on the basis of dead cells count present in the microscopic images. The algorithm takes a few seconds to run and the overall accuracy of the proposed algorithm was found to be approx. 97% and 83% for different sets of images. The various image peculiarities which led to error include high cells clustering, poor contrast, and noisy background.

**Keywords:** Nanotechnology, Nanocarriers, Drug Delivery System, Toxicity, Image Processing

Received on 07 January 2019, accepted on 16 February 2019, published on 19 February 2019

Copyright © 2019 B. Saini *et al.*, licensed to EAI. This is an open access article distributed under the terms of the Creative Commons Attribution licence (<http://creativecommons.org/licenses/by/3.0/>), which permits unlimited use, distribution and reproduction in any medium so long as the original work is properly cited.

doi: 10.4108/eai.13-7-2018.156593

\*Corresponding author. Bhavna.saini@jaipur.manipal.edu

### 1. Introduction

Nanotechnology has prominently advanced in biomedical applications such as drugs/ gene delivery systems, probing of DNA structure, tissue engineering etc. with the utilization of nanoparticles (NP). One of the main reasons for using these nanoparticles in therapeutic applications is their small size [1, 2] that makes them eligible for fast absorption and release behaviour of bioactive molecules including drugs. Moreover, NPs surfaces and size features can be costumed and controlled in a desirable manner which is a prime factor behind their popularity in the biomedical community. The prevailing synthetic organic chemistry has begun a new pathway to design these nanomaterials (NM) using different chemical compositions, diverse material resources, and various synthetic routes. All these advancements have resulted in

a breakneck increment in the requirement of various types of nanomaterials in biological applications. Inclusive of various compelling properties and features, the use of nanomaterials also gives rise to various harmful effects not only for human but for the environment also [4]. The small size of NM exposes their large surface area to cellular units that can lead to some toxic effects.

#### 1.1 Drug Delivery System: Methods and Challenges

Drug delivery system is one of the most popular biological applications that make use of several nanomaterials and nanostructures [3]. Drug delivery system refers to a therapeutic process in which an appropriate amount of pharmaceutical compound or drug is transferred to the body to have the desired physiological effects. The main aim of a drug delivery system is to

successfully integrate drug into nanocarriers and ensure that this integration has transported an adequate amount of drug to diseased sites [3-6]. One of the best examples of this kind of therapeutic systems is chemotherapy, which is used to treat cancer and tumors. The major chemical compounds for chemotherapeutics cannot be utilized directly due to their solubility and toxicity issues as an excess dose of the drug may cause severe physiological discomforts. To address these issues, a wide variety of biopolymer are used as carriers in controlled drug delivery technology. Most of these promising biopolymers are completely non-toxic, non-carcinogenic, easily available, and economically viable, water soluble and this is the reason why they are so popular in medicines and pharmacy. Among various methods of preparation of nanoparticles of the biopolymer, emulsion crosslinking is one of the efficient techniques that make use of certain crosslinking agents for biopolymers to make them insoluble in water [7, 8]. In fact, biopolymers are not toxic in nature, but the use of chemical crosslinking agents may cause toxicity in the prepared nanoparticles. Another crucial situation that normally arises during the stabilization of NM for the drug delivery process is the use of a reducing agent that may contribute significantly to overall toxicity. Besides biopolymer based nanoparticles, superparamagnetic nanoparticles have also emerged as exceptional nanomedicine due to their unique physical properties and ability to act at molecular and cellular levels of biological interaction. The unique characteristics of these nanoparticles enable them as next-generation carriers for drug delivery system. However, while devising the superparamagnetic nanocarriers, toxicity evaluation is one of the main prospects that need to figure out prior to clinical applications. For designing a drug delivery system the toxicity is one of the key issues to be addressed seriously as the clinical trials are not much successful due to undetected toxic effects of employed nanomaterials [5]. Hence, there is an urgent need to explore a mechanism that may rationally predict the toxic nature of these NM in well advance to their eventual applications.

## 1.2 Motivation

This toxic nature of nanoparticles can't be neglected and must be properly addressed. Thus being motivated by the prediction potential of cytotoxicity pertaining to nanocarriers, the objectives of the present work include identifying the toxic nature of some gelatin based nanocarriers that have been previously investigated as drug delivery nanocarriers. The toxicity prediction was performed on the basis of microscopic images generated during drug delivery process and validated by the experimental findings.

Computational evaluation of biological images has attracted a great interest of researchers worldwide with the introduction of machine learning techniques. Identifying significant and functionality related features that appropriately characterize the regularities or sequence

inherent in biological image data plays an important role in future predictions. Digital image processing makes this task more quick and decisive by means of automatic processing, manipulation and analysis [29].

## 2. EXPERIMENTAL

### 2.1 Materials

Gelatin used as biopolymer for preparation of nanocarriers was supplied by Loba Chemie, India. Glutaraldehyde was used as a crosslinking agent for gelatin and purchased from Loba Chemie, India and used without further purification. Other chemicals such as toluene (for preparing oil phase) and acetone were of analytical purity grade.

### 2.2 Methods

#### 2.2.1 Preparation of gelatin nanocarriers

The gelatin nanocarriers were prepared by emulsion crosslinking method as described elsewhere [7]. In a typical experiment, 2 g of gelatin was dissolved in 20 mL hot water under mild stirring for 1 h till the complete dissolution of gelatin. Now to this aqueous solution of gelatin, a definite volume of toluene was added with vigorous stirring so that a stable emulsion of gelatin was obtained. Now a 1:1 (v/v) mixture of toluene and glutaraldehyde was prepared with constant stirring and added to the gelatin emulsion with pre-determined rate. The crosslinking of gelatin with glutaraldehyde was allowed to take place for 6 h till the color of gelatin starts changing from slight yellow to dark brown which was an indication of crosslinking of gelatin by glutaraldehyde. After completion of the crosslinking reaction the gelatin nanoparticles were filtered, washed thoroughly with acetone and water and dried. The dried gelatin nanoparticles were stored in air-tight containers for further study.

#### 2.2.3 In vitro toxicity of gelatin nanoparticles

In in-vitro methods, toxicity is judged on the basis of fastening of cells. If a chemical compound is capable of modifying the morphology of cells, then it unfavorably influences the cell growth and causes the cell death. To examine in-vitro cytotoxicity of the as prepared glutaraldehyde crosslinked gelatin nanoparticle, the extract method (ISO – 1099 33-5) on L 929 fibroblast cells has been widely used [9]. In this method, the powdered material is immersed in culture medium with serum and then the extract is build up by incubating the pre penetrated test material with serum for 24 h. After incubation process, the extract is filtered and diluted with culture medium to get required concentration. Later on

after dilution of test sample extract, positive control and negative control are investigated microscopically for cellular reaction. The microscopic images indicate the toxicity behavior. The toxicity levels such as mild, moderate and severe are determined using the counts of live and dead cells shown in the microscopic images. Manual count of these cells can lead to error. Therefore, the tool of image processing can be successfully and precisely used for accurately calculating the drug potency and toxicity of chemical compounds, which act as promising drug candidate.

## 2.3 Proposed Algorithm

Automated detection of cells is nowadays a quite studied field, for which enormous number of methods has been defined, and study of new algorithms is still going on [16-19]. This paper focuses on relatively new or undiscovered area, where cell detection and estimation plays an important role in toxicity prediction of drug delivery nanocarriers. The algorithm used in the present study for morphological evaluation of cytotoxicity is shown in Fig. 1.

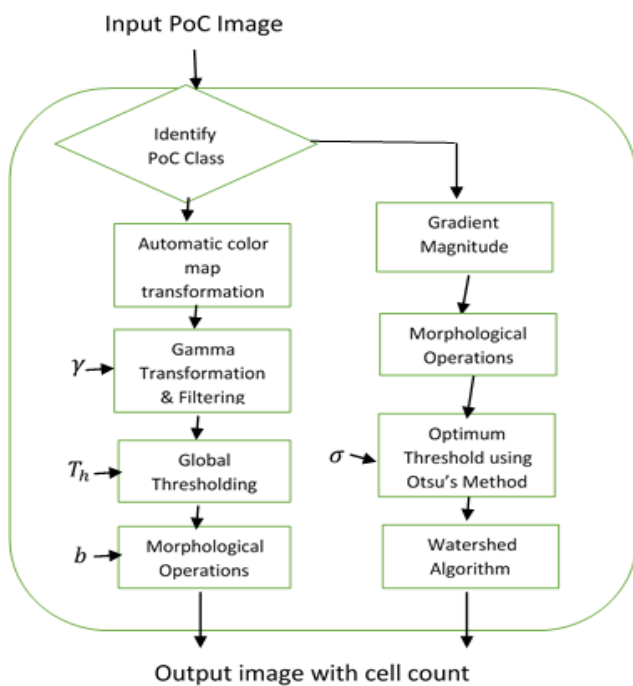


**Figure 1.** Flowchart summarizing the main steps of proposed algorithm for positive control images processing

## 3. IMPLEMENTATION AND RESULTS

Initially, the vitro cytotoxicity test is performed on L-929 fibroblast cells. The reactivity of test and control samples is evaluated through three test control

microscopic images which are: positive control, negative control and test sample. These control samples acquire some grade values which determine the toxic nature. The sample with grade value 4 is severely reactive while the sample with grade 0 tends to be non-reactive or non-toxic. The sample microscopic images are the 2D forms of 3D samples, which becomes a major challenge while extracting the correct number of cells out of it. The correct cell count can interpret the correct toxic nature of drug sample. In this paper, we have focused only on positive control images and test sample images.

As the input 2D images have cell appearance either in embossed or textured form, they are categorized into two classes' class1-PoC (Positive control image) and class2-Poc. Figure 2(a) and 2(b) shows the difference between these two classes of images. Different algorithms are defined for Class-1 PoC and Class-2 POC according to their texture. Next section discusses the algorithm applied.

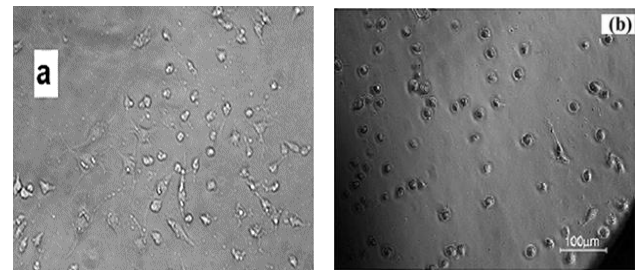


**Figure 2.** (a) Positive control Class-1 Image and (b) Positive Control Class-2 Image

### 3.1 Positive Control Class-1 images (PoC)

**Color Map Transformation:** The first step of processing the positive control sample is the linear association of red, blue and green color channel of input image. This transformation is done for the smooth and adaptable processing of image and is based on individual weights associated with each color channel. This resultant brought out image is in grayscale form.

$$I(x, y) = W_r \cdot I_r(x, y) + W_g \cdot I_g(x, y) + W_b \cdot I_b(x, y) \quad |$$

$$\text{where } W_r + W_g + W_b = 1,$$

$$W_r, W_g, W_b \geq 0$$

(1)

**Gamma Transformation:** The grey value of these images are not evenly distributed and having high contrast. To divulge the image characteristics, the pixel intensity values are transformed using filtering techniques. Several approaches previously proposed in

literature includes histogram equalization, decision based median filter and adaptive fuzzy switching weighted median filter which have high computational complexities [10]. Enhancement of images can be classified into global, local and hybrid. Global enhancement follows a single function for each pixel transformation which can lead to over or under enhancement of image. Hence here we have taken up a hybrid approach that begins with gamma transformation which afterwards filtered using entropy based filter.

For the initial enhancement of images, the contrast of images was built up. For this, an outlining technique has been applied on images  $I(x,y)$  from low to bottom and high to top. The grey scale is curved to brighten the intensity level and further implemented a gamma transformation on it. As gamma value ranges from 0 to 1, we have tried various values and find out the optimum one for our images.

$$I(x,y) = I_{max}(x,y) * \left[ \frac{(I(x,y) - I_{min}(x,y))^\gamma}{(I_{max}(x,y) - I_{min}(x,y))^\gamma} \right]$$

Where  $0 < \gamma < 1$  (2)

The impact of variation in  $\gamma$  value can be explained from Figure 3, where the outcome of some sample  $\gamma$  values has been shown. With  $\gamma = 0.3$ , the cell pixels' intensity level is not much differentiated from that of background intensity. The increase in  $\gamma$  value leads to more enhancement such that the cells lying in the boundary also seems to be more visible. As it can be seen in Fig 3,  $\gamma = 0.9$  brought the image to the required form, where the cells are properly visible. Hence our algorithm works with  $\gamma = 0.9$ .

Further the edges are attenuated by illuminating pixels with diverse neighborhood. It scales every pixel of the current image identical to entropy measure of pixel value of its given neighborhood.

$$I_e(x,y) = N \left[ \sum_{i=1}^n I_i * \text{Log}_2 \right]$$
 (3)

The window size of neighbourhood is considered as 9x9 for filtering.

**Binary conversion:** Structuring element is one of the key requirements for morphological operations to be implemented on the input images. Structuring element is basically binarization of the image which is transferred over the target image. Binarization process isolates background pixels from foreground pixels based on the threshold value of luminance. Clustering based, histogram based are the generally known thresholding methods [11-13]. More progressive methods include graph cut and level set based, but these lead to more computational complexity [12, 14, 15].

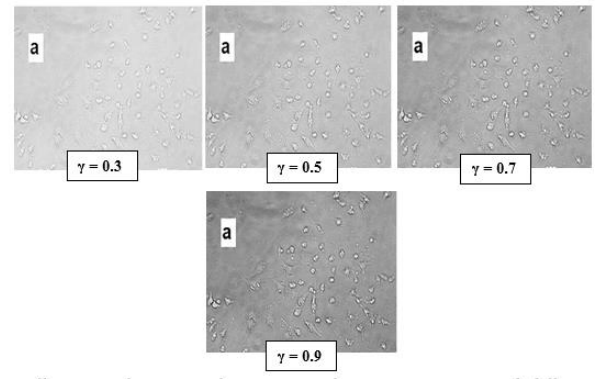


**Figure 3.** Illustrating the impact of Gamma transformation on images with different gamma values

Here a basic thresholding method was applied where pixels in input image having luminance value greater than threshold value are replaced with value 1, while rest of the pixels is replaced with value 0.

$$I(x,y) = \begin{cases} 1, & I_e(x,y) \geq T_h \\ 0, & \text{Otherwise} \end{cases}$$

where  $T_h = \text{threshold value}$  (4)

Figure 4 shows the different outcomes of image threshold. Here  $T_h=0.8$  proves to be optimal threshold, as most of the cells are clearly recognizable which makes the further process of cell information retrieval more smooth.

**Morphological Opening Operations:** Morphological operations have the capability to excerpt the desired components from the images. The opening morphological operation is an erosion process trailed by dilation method. Erosion method determines the locus of points attained by the centre of structuring element when it superimposes the binary image.

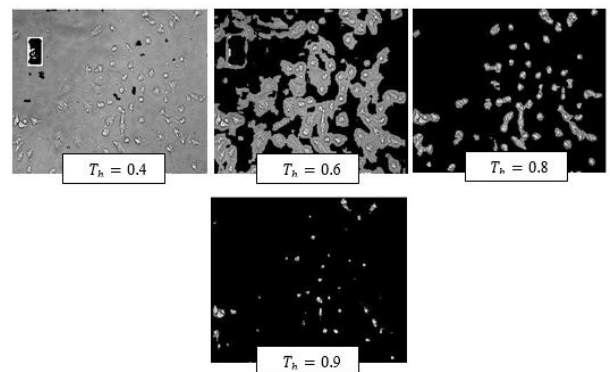


**Figure 4.** Images illustrating the outcomes after Binarization process with different threshold values

Here erosion is performed on image  $I$  with structuring element  $b(x)$  to find the minimum of neighbourhood points.

$$\begin{aligned}
 I &= (I \ominus b)(x) \\
 &= \infimum_{y \in B} [I(x + y) - b(y)]
 \end{aligned}
 \tag{5}$$

Where  $B$  is bound space.

After completion of erosion process, the dilation process is performed where binary image  $I$  and kernel value (Structuring element) are taken as inputs. The image  $I$  is dilated using kernel  $k$  which results in confine aggrandizement of foreground pixel i.e. the size of foreground pixels were evolved while neighbourhood holes were narrowed. The accurate impact of this operation comes with the kernel value defined. The kernel value  $k(x)$  is defined as

$$k(x) = \begin{cases} 0, & x \in B \\ -\infty, & \text{Otherwise} \end{cases}$$

where  $B \subseteq E$

where  $B = \text{bounded space}$ ,  $E = \text{grid}$

Dilation process is the intersection of  $I_o$  (origin of binary image  $I$ ) and  $k$  such that it has a non-empty set of Euclidean coordinates correspondent to input binary image.

$$\begin{aligned}
 (I \oplus k)(x) &= \supremum_{y \in E} [I(x) + k(x - y)] \\
 &= \supremum_{z \in E} [I(x - z) + k(z)] \\
 &= \supremum_{z \in B} [I(x - z)]
 \end{aligned}
 \tag{7}$$

The results after this operation can be explained from Fig. 5.

After that close operation is performed which is basically dilation process followed by erosion. This process removes the small holes or noise present in the image.

$$(I \odot k)(x) = (I \oplus k) \ominus k \tag{8}$$

After this operation the image produced was in the required format, using which the count of dead cells was identified. The count of these dead cells in the positive control image shows the toxicity severity level. The analysis was performed on total 15 Class-1 PoC images and the results were quite accurate, Table 1 shows the result of all images and Fig 11 shows the ROC curve for the same

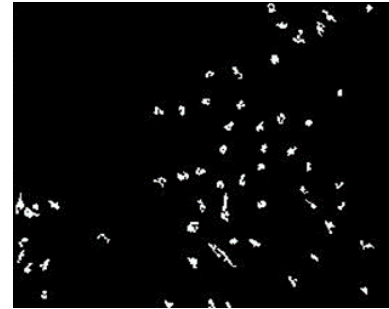


**Figure 5.** Morphological Operation Result

It is imperative for this framework to be able to identify the correct number of cells with extreme certainty. The aim of this study is to develop system with sheer automation and least human effort. While this method works well with class 1 positive control images, as expected, it was not withstanding adequate for class 2 positive control images [20]. As depicted in fig.6 the cells in class 2 image are not well recognized by this method. In particular, this procedure performs well when boundaries are smooth. In class2 PoC images the boundaries are noisier and applying this method results in over segmentation. Overcoming this concern requires a more control over pre-processing values.



**Figure 6.** Depicting the outcome of Class2 PoC image when algorithm of PoC 1 Class was applied..

Our method to carry out this is built on appropriate morphological pre-processing and segmentation. The method for class2 positive control images ensue as follows:

### 3.2 Positive Control Class-2 images (PoC)

Initially discontinuity in intensity value is identified, depending upon the direction of maximum intensity variation, unit vector, base image position and the change in contrast of local image along normal. The values of gradient magnitude have been find out at each pixel by convolving image with horizontal and vertical derivative filters.

#### Gradient Vector

$$\nabla I = \left[ \frac{\partial I}{\partial x}, \frac{\partial I}{\partial y} \right]^T$$

Where  $\tau$  = Threshold Value using sobel kernel

$$\partial x = f(x + n, y) - f(x - n, y)$$

$$\partial y = f(x, y + n) - f(x, y - n)$$

Where  $n$  = small integer value (9)

#### Magnitude

$$|\nabla I| = \sqrt{\left(\frac{\partial I}{\partial x}\right)^2 + \left(\frac{\partial I}{\partial y}\right)^2} \quad (10)$$

#### Orientation

$$\theta = \alpha \tan\left(\frac{\partial I}{\partial x}, \frac{\partial I}{\partial y}\right) \quad \text{Where } \alpha = \text{arc} \quad (11)$$

The previous method results in accurate gradient results. Fig 7(a) shows an example of the outcome obtained.

#### Generating Structuring Element

A flat structuring element  $S_L$  was generated symmetrical to adjacent centres. The  $S_L$  was further used to dilate the images. Grayscale dilation process had been carried out to widen the foreground objects of the image so that it can be helpful in easy cell detection.

$$(I \oplus S_L)(x, y) = \max\{A(x - x', y - y') + S_L(x', y') | (x', y') \in D\} \quad (12)$$

As we are using a flat structuring element, hence

$$S_L(x', y') = 0 \text{ And}$$

$$(I \oplus S_L)(x, y) = \max\{A(x - x', y - y') + (x', y') \in D\} \quad (13)$$

To make the cell appearance more clear, hole filling is done

$$F(x, y) = \begin{cases} 1 - I(x, y) & \text{If } (x, y) \text{ is on the border of } I \\ 0 & \text{Otherwise} \end{cases} \quad (14)$$

The effect of using dilation process followed by hole filling is illustrated in Fig 7(b). As it can be seen the cells becomes easily detectable now. But to enhance it more and to remove the noise, a filtering process was done.

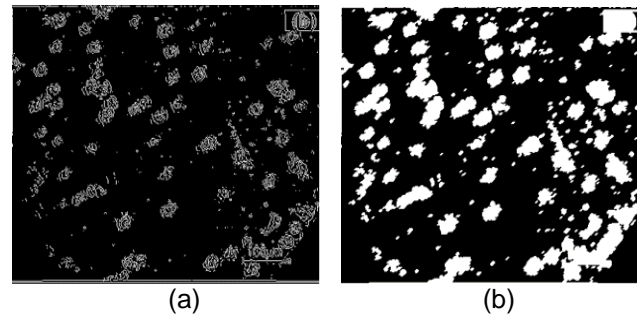


Figure 7. (a) Illustrates the effect of applying gradient vector on the image and (b) the image after hole filling process.

#### Top-hat Filtering

Morphological Opening was performed using the structuring element, which extracts the small components and details from the given image. It is performed as difference between input image  $I$  and structuring element

$$I_w(f) = f - S_L \quad (15)$$

Fig 8 shows the outcome of the above function.

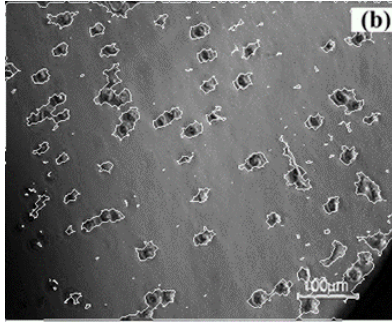


**Figure 8:** Results after morphological operation

Most of the cells in the image got detected but still the count was not correct. This difference in the count occurred due to closely connected cells, which were considered as one object. Fig 9(a) illustrates an example of connected cells scenario. The cell segmentation is one of the crucial and important part of the process. One of the classical method for segmentation used in the past is Watershed Algorithm [23][24]. Various improvements and variations of this method were generated and utilized due to its simplicity, speed and easily adjustable distance map factor [22][25][26].

$$\sigma_w^2 = v_1(t)\sigma_1^2(t) + v_2(t)\sigma_2^2(t)$$

Where  $v$  is the class probability of different grey level pixels

And value of  $v$  is given by:

$$v_1(t) = \sum_{i=0}^t P(i) \text{ and } v_2(t) = \sum_{i=0}^{255} P(i)$$

Total variance is calculated as

$$\sigma_2 = \sigma_w^2(t) + \sigma_b^2(t)$$

Where  $\sigma_w^2(t)$  = within class variance

$$\sigma_b^2(t) = \text{between class variance} \quad (16)$$

After finding the threshold values, the watershed segmentation was applied. The cell segmentation has been performed using the distance transform method of watershed. Initially the distance has been calculated from each pixel to its nearest neighbour pixel having non zero values.

Let  $P$  be the set of points in space  $Z$ . For every point  $p$  of  $P$ , the distance  $d(p)$  of  $p$  to the corresponding set  $P^c$  is defined as:

$$\forall p \in P, d(p) = \text{dist}(p, P^c) \quad (17)$$

Where  $\text{dist}(p, P^c)$  is the distance of  $p$  to the nearest point  $P^c$

A section of distance  $d$  at level  $i$  is defined by:

$$Y_i(d) = \{p: d(p) \geq i\} = P \ominus D_i \quad (18)$$

Where  $D_i$  is a disk of radius  $i$ . The distance segmentation method resulted in suitable partition of the connected cells. Fig 9(b) illustrated the outcome with an example.

The algorithm was tested on total 15 Class-2 PoC images and it works with approx. 97% accuracy. Table 2 illustrates the result of all images and Fig 12 shows the ROC curve for the same.

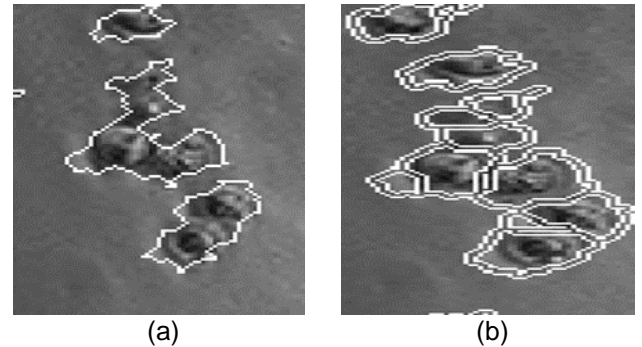


**Figure 9:** (a) Clustered cells (b) Cells after segmentation

### 3.2 Test Sample

Test sample images are the outcome of drug formation test sample. As the texture of such images is different from that of positive control images as shown in Fig 10(a), the processing techniques will also have variations. Primary phase of processing the test sample images is conversion of RGB channel to gray level. Further sharpening is done to enhance the edges and other image components with high frequency. The low pass component of input image is captured as unsharp version  $I_{unsharp}(x, y)$  of image which is then subtracted from input test sample image  $I(x, y)$ .

$$f(x, y) = I(x, y) - I_{unsharp}(x, y)$$

$$f_{sharp}(x, y) = I(x, y) + (k * f(x, y)) \tag{19}$$

More enhancement of the image is done by utilizing the factor k, which is a numerical value derived as standard deviation of Gaussian low-pass filter. This value executed as radius, which holdback the area about the edge pixels that are influenced by sharpening process. The value of this k can be calculated as

$$g(x, y) = \frac{1}{2\pi\sigma^2} e^{-\frac{x^2+y^2}{2\sigma^2}}$$

where  $\sigma$  = Std. Dev of Gaussian (20)

**Hough Transformation:** Discovering the occurrence of dead cells with variant class of shapes, present in the test sample image, though transformation was adapted [28]. A voting procedure is performed in the set of all possible association of values. The procedure is followed for all different parameter values present in the model.

$$x = a + (r \times \cos \theta)$$

$$y = b + (r \times \sin \theta)$$

Where  $a, b$  = center and  $r$  = radius (21)

The results of test sample image process have been shown in fig 10(b). Here the blue circle shows the dead cells detection.

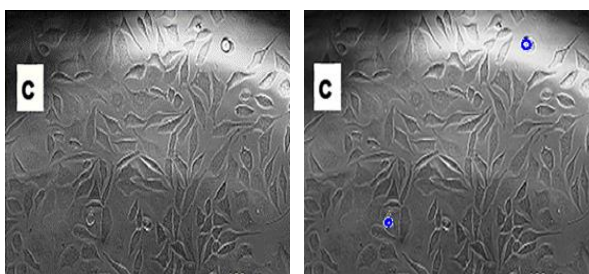


**Figure 10:** (a) The test sample image and (b) Image illustrates the final outcome with dead cell highlighted

#### 4. MODEL EVALUATION MEASURES

The correctness of the model was evaluated on the basis of correctly identified and not identified instances. The precision and recall metrics [29][30] were computed as:

$$Precision = \frac{TP}{(TP + FP)} \tag{22}$$

Where  $TP$  = Accurately Identified Cells  
 $FP$  = Undetected Cells

$$Recall = \frac{TP}{(TP + FN)} \tag{23}$$

Where  $FN$  = incorrectly identified or intruded cells

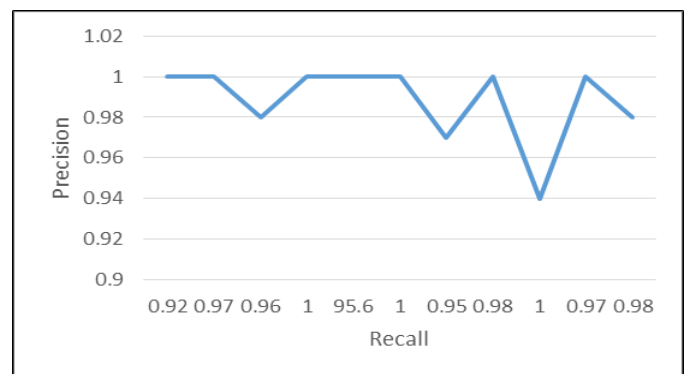


**Figure 11.** ROC Curve for PoC Class- 1 Images

Table 1: Positive control images Class 1 results

Image ID	No. of Cells	of Accurately Identified Cells	Undetected Cells	Intruded Cells	Precision	Recall
1	52	50	2	0	1.00	0.92
2	35	34	1	0	1	0.97
3	64	62	1	1	0.98	0.96
4	60	60	0	0	1	1
5	46	44	2	0	1	95.6
6	68	68	0	0	1	1
7	45	42	2	1	0.97	0.95
8	60	59	1	0	1	0.98
9	55	52	0	3	0.94	1
10	37	36	1	0	1	0.97
11	65	64	1	0	0.98	0.98
12	47	45	2	0	1	0.95
13	68	67	0	1	0.98	1
14	52	52	0	0	1	1
15	56	55	0	1	0.98	1
Total	810	790	13	7	0.98	0.97
Percentage		97.5%	1.6%	0.8%		

Table 2: Positive control images Class 2 results

Image ID	No. of Cells	of Accurately Identified Cells	Undetected Cells	Intruded Cells	Precision	Recall
1	68	67	1	0	1	0.98
2	64	64	0	0	1	1
3	66	65	0	1	0.98	1
4	47	47	0	0	1	1
5	38	37	1	0	0.97	1
6	36	34	1	0	1	0.97
7	37	35	0	2	0.95	1
8	46	43	3	0	0.93	1
9	64	59	3	2	0.96	0.95
10	68	67	1	0	1	0.98
11	64	62	2	0	1	0.96
12	60	58	0	2	0.96	1
13	72	69	0	2	0.97	1
14	45	45	0	0	1	1
15	65	62	1	2	0.96	0.98
Total	840	814	13	11	0.97	0.98
Percentage		96.9%	1.5%	1.3%		

Table 3: Test sample Image results

Image ID	No. of Cells	Accurately Identified Cells	Undetected Cells	Intruded Cells	Precision	Recall
1	11	9	0	2	1	0.81
2	3	3	0	0	1	1
3	5	4	0	1	1	0.80
4	12	10	1	1	1	0.83
5	5	4	1	0	1	0.80
Total	36	30	2	4	1	0.86
Percentage		83.3%	5.5%	11.1%		

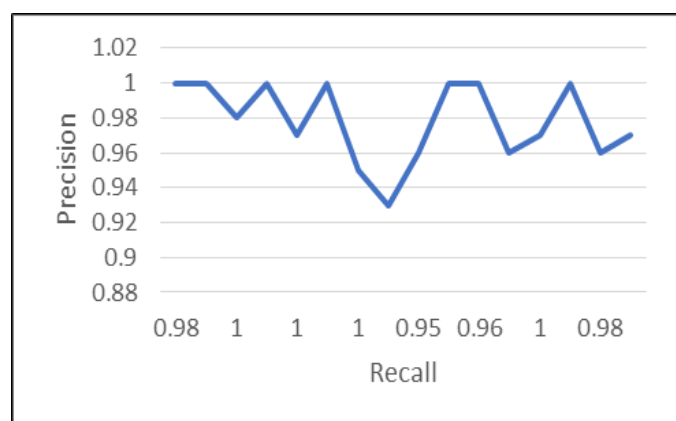


Figure 11. ROC Curve for PoC Class- 2 Images

## 5. CONCLUSION

The current study has developed an image analysis framework which could possibly be utilized for regular toxicity determination of a compound in drug delivery system. Previous analysis consists of distinct approaches for automatic cell detection, but to the best of our knowledge there is no work done for toxicity prediction of a drug delivery system based on this. Here

we have collected a set of 25 sample images from different sources including Department of Chemistry, Govt. Autonomous Science College, Jabalpur (MP), INDIA, research studies and web sources. The variants of the proposed algorithm were applied based on the type of control sample images. For validation of the outcome, initially all the images were inspected and evaluated manually and the results generated from our automated framework were captured. We have followed a conservative assessment approach which compares the outcome of both manual cell count and the count generated from proposed automatic framework. Table 1, Table 2 and Table 3 summarized the result analysis which contains few cases of undetected and intruded cells. Undetected cells are those which are usually less textured or the shape of cells is quite constrict. The prime mover of intruded cells error is the merging of two or more cells into a cluster with infirm boundaries. To some extent, the choice of parameter values is the cause of these errors. While performing this assessment, one of the key point which was observed is the difference of processing time. While counting manually it takes around 30 sec to 1 min, which varies from person to person ability. On the other side, the proposed system works only in few seconds from 5 to 10 seconds. This difference in time doesn't matter when we talk about few 10 -20 images, but in case of 100s of images, it matters a lot. Apart from this, there occur chances of counting error while doing it manually

which can be minimized on automatization. The proposed algorithm works well and prove to be robust and accurate. The accuracy of counted cells helps in accurate toxicity detection.

## References

- [1] Alagarasi, A. (2011). Introduction to nanomaterials. National Center for Environmental Research.
- [2] Abhilash, M. (2009). Potential Applications of Nanoparticles.
- [3] Lehner, R., Wang, X., Marsch, S., & Hunziker, P. (2013). Intelligent nanomaterials for medicine: carrier platforms and targeting strategies in the context of clinical application. *Nanomedicine: Nanotechnology, Biology and Medicine*, 9(6), 742-757.
- [4] Agarwal, M., Murugan, M. S., Sharma, A., Rai, R., Kamboj, A., Sharma, H., & K Roy, S. (2013). Nanoparticles and its toxic effects: A review.
- [5] Fischer, H. C., & Chan, W. C. (2007). Nanotoxicity: the growing need for in vivo study. *Current opinion in biotechnology*, 18(6), 565-571.
- [6] Tiwari, G., Tiwari, R., Sriwastawa, B., Bhati, L., Pandey, S., Pandey, P., & Bannerjee, S. K. (2012). Drug delivery systems: An updated review. *International journal of pharmaceutical investigation*, 2(1), 2.
- [7] Pal, A., Bajpai, J., & Bajpai, A. K. (2018). Easy fabrication and characterization of gelatin nanocarriers and in vitro investigation of swelling controlled release dynamics of paclitaxel. *Polymer Bulletin*, 1-21.
- [8] Khan, H., Shukla, R. N., & Bajpai, A. K. (2016). Genipin-modified gelatin nanocarriers as swelling controlled drug delivery system for in vitro release of cytarabine. *Materials Science and Engineering: C*, 61, 457-465.
- [9] ISO 10993-5: Biological evaluation of medical devices—Part 5: Tests for in vitro cytotoxicity. Arlington, VA: ANSI/AAMI; 1999.
- [10] Sezgin, M., & Sankur, B. (2004). Survey over image thresholding techniques and quantitative performance evaluation. *Journal of Electronic imaging*, 13(1), 146-166.
- [11] Garg, N. (2013). Binarization Techniques used for grey scale images. *International Journal of Computer Applications*, 71(1).
- [12] Chen, X., & Pan, L. (2018). A Survey of Graph Cuts/Graph Search based Medical Image Segmentation. *IEEE Reviews in Biomedical Engineering*.
- [13] Guo, R., & Pandit, S. M. (1998). Automatic threshold selection based on histogram modes and a discriminant criterion. *Machine Vision and Applications*, 10(5-6), 331-338.
- [14] Lie, J., Lysaker, M., & Tai, X. C. (2006). A binary level set model and some applications to Mumford-Shah image segmentation. *IEEE transactions on image processing*, 15(5), 1171-1181.
- [15] Leskó, M., Kato, Z., Nagy, A., Gombos, I., Torok, Z., Vigh Jr, L., & Vigh, L. (2010, August). Live cell segmentation in fluorescence microscopy via graph cut. In *Pattern Recognition (ICPR), 2010 20th International Conference on* (pp. 1485-1488). IEEE.
- [16] Xing, F., & Yang, L. (2016). Robust nucleus/cell detection and segmentation in digital pathology and microscopy images: a comprehensive review. *IEEE reviews in biomedical engineering*, 9, 234-263.
- [17] Di Ruberto, C., Dempster, A., Khan, S., & Jarra, B. (2002). Analysis of infected blood cell images using morphological operators. *Image and vision computing*, 20(2), 133-146.
- [18] Ambriz-Colin, F., Torres-Cisneros, M., Avina-Cervantes, J. G., Saavedra-Martinez, J. E., Debeir, O., & Sanchez-Mondragon, J. J. (2006, November). Detection of biological cells in phase-contrast microscopy images. In *Artificial Intelligence, 2006. MICAI'06. Fifth Mexican International Conference on* (pp. 68-77). IEEE.
- [19] Byun, J., Verardo, M. R., Sumengen, B., Lewis, G. P., Manjunath, B. S., & Fisher, S. K. (2006). Automated tool for the detection of cell nuclei in digital microscopic images: application to retinal images. *Mol Vis*, 12(105-07), 949-60.
- [20] Atteya, M. A., Salem, M. A. M. M., Hegazy, D. A. K. M., & Roushdy, M. I. (2016). Image segmentation and particles classification using texture analysis method. *Research on Biomedical Engineering*, 32(3), 243-252.
- [21] Somasundaram, K., & Kalaiselvi, T. (2010). A method for filling holes in objects of medical images using region labeling and run length encoding schemes. In *National Conference on Image Processing (NCIMP)* (pp. 110-115).
- [22] Ortiz De Solórzano, C., Garcia Rodriguez, E., Jones, A., Pinkel, D., Gray, J. W., Sudar, D., & Lockett, S. J. (1999). Segmentation of confocal microscope images of cell nuclei in thick tissue sections. *Journal of Microscopy*, 193(3), 212-226.
- [23] Lin, G., Adiga, U., Olson, K., Guzowski, J. F., Barnes, C. A., & Roysam, B. (2003). A hybrid 3D watershed algorithm incorporating gradient cues and object models for automatic segmentation of nuclei in confocal image stacks. *Cytometry Part A*, 56(1), 23-36.
- [24] Mackin, J. R., Newton, L. M., Turner, J. N., & Roysam, B. (1998). Advances in high-speed, three-dimensional imaging and automated segmentation algorithms for thick and overlapped clusters in cytologic preparations. Application to cervical smears. *Analytical and quantitative cytology and histology*, 20(2), 105-121.
- [25] Al-Kofahi, Y., Lassoued, W., Lee, W., & Roysam, B. (2010). Improved automatic detection and segmentation of cell nuclei in histopathology images. *IEEE Transactions on Biomedical Engineering*, 57(4), 841-852.
- [26] Wang, Y., Zhang, Z., Wang, H., & Bi, S. (2015). Segmentation of the clustered cells with optimized boundary detection in negative phase contrast images. *PLoS one*, 10(6), e0130178.
- [27] Otsu, N. (1979). A threshold selection method from gray-level histograms. *IEEE transactions on systems, man, and cybernetics*, 9(1), 62-66.
- [28] Smereka, M., & Dulęba, I. (2008). Circular object detection using a modified Hough transform. *International Journal of Applied Mathematics and Computer Science*, 18(1), 85-91.
- [29] Sharma, M., Sharma, S., & Singh, G. (2018). Performance Analysis of Statistical and Supervised Learning Techniques in Stock Data Mining. *Data*, 3(4), 54.
- [30] Sharma, M., Singh, G., & Singh, R. (2017). Stark Assessment of Lifestyle Based Human Disorders Using Data Mining Based Learning Techniques. *IRBM*, 38(6), 305-324.